

Modeling Requirements for Analysis and Optimization of JVX Proprotor Performance

C. W. Acree, Jr.
 Aeromechanics Branch
 NASA Ames Research Center
 Moffett Field, California
 Cecil.W.Acree@NASA.gov

Abstract

Existing tiltrotors are based on technology dating back 25 years or more. Present-day analytical and design methods promise useful improvements in performance compared to what was then possible. This paper applies CAMRAD II to proprotor performance optimization with different levels of analytical sophistication, ranging from simple momentum theory and combined blade-element/momentum theory to prescribed- and free-wake models; rigid and elastic blade models are also examined. Variations in blade twist distribution, solidity, taper, sweep and droop are explored. The purpose of the research is to determine the minimum requirements for analytical methodologies for successful optimization. Although the design of an improved rotor is not the immediate objective, design improvements naturally result and so are also discussed. The results of the study will be used to guide research directions in such areas as coupled CFD/CSD and improved sizing codes.

Notation			
JVX	Joint Vertical Experimental	P	rotor power
LCTR	Large Civil Tiltrotor	r	local blade radius
NFAC	National Full-Scale Aerodynamics Complex	r_{ds}	transition radius for droop or sweep
OARF	Outdoor Aerodynamic Research Facility	R	rotor radius
PTR	Propeller Test Rig	R'	projected radius
		T	rotor thrust
A	rotor disk area	v_0	induced velocity in axial flow
K_L	stall-delay factor (Corrigan model)	v_h	induced velocity in hover
K_{sdD}	stall-delay factor for drag (Selig model)	v_i	local induced velocity
K_{sdL}	stall-delay factor for lift (Selig model)	V	flight speed (rotor axial velocity)
c	blade chord	V_{tip}	rotor tip speed
c_d	airfoil section drag coefficient	V_{tun}	wind-tunnel airspeed
c_{dL}	linear approximation of drag coefficient	x	in-plane offset due to sweep
c_{dtable}	drag coefficient from airfoil table	z	out-of-plane offset due to droop
c_{dz}	drag coefficient at zero lift	α	angle of attack
c_l	airfoil section lift coefficient	α_z	zero-lift angle of attack
$c_{l\alpha}$	lift curve slope (linear)	η	propulsive efficiency, T/P
c_{lL}	linear extension of lift coefficient	κ_λ	factor on induced velocity
c_{htable}	lift coefficient from airfoil table	μ	advance ratio, V/V_{tip}
C_T	rotor thrust coefficient, $T/(\rho A V_{tip}^2)$	Ω	rotor rotational speed
FM	rotor hover figure of merit, $(T\sqrt{T/2\rho A})/P$	ρ	air density
M_{tip}	rotor tip Mach number	σ	rotor solidity, $Nc/\pi R$
N	number of blades	τ	local blade twist

Scope of Research

Presented at the AHS 64th Annual Forum, Montréal, Canada, April 29-May 1, 2008. This material is declared a work of the U. S. Government and is not subject to copyright protection.

The research reported here evolved from the NASA Heavy Lift Rotorcraft Systems Investigation (Ref. 1). That study selected the Large Civil Tiltrotor (LCTR) as having the best potential of several configurations to meet

NASA technology goals, which were chosen to stimulate advanced VTOL technology development. With a tiltrotor selected as the preferred concept, research turned towards advanced proprotor designs.

Reference 2 examined the effects of tip speed, blade number, and other top-level design parameters on LCTR rotor size, vehicle gross weight, and cost (see also Ref. 1). Reference 3 optimized twist, taper and precone for the resulting rotor design, examined the benefits of new airfoils to rotor performance, and explored the aeroelastic stability (whirl flutter) of the complete aircraft. In contrast, the present effort focuses on the details of rotor performance optimization by extending the methods of Ref. 3 to a wider variety of design parameters, with the JVX test rotor as the baseline.

Because proprotors have higher twist and lower aspect ratio than conventional helicopter rotors, it is worthwhile to re-examine the analytical tools used to predict rotor performance and the test data used to validate the methodology. The critical criterion for design optimization is that the procedure must indicate the correct values of the parameters being optimized, not that the maximum values of performance be perfectly predicted. The present study applies the analyses validated in Ref. 4 to coupled hover/cruise performance optimization, with the goal of determining minimum requirements for the aeromechanics analyses that underlie the optimization process. There is also an implied tradeoff between accuracy and computational time. The focus of the research is, therefore, different than that of (e.g.) Refs. 5 and 6, although those two papers make for interesting contrasts in their approaches to proprotor optimization.

Aerodynamic analysis is here emphasized over structural analysis because of the former's relatively lower level of maturity and greater impact on computational resources. The focus here is on the predictive methodology, not the optimization process or final design. The larger purpose is to guide future research, including experimental tests, by providing a rational basis for setting priorities.

CAMRAD II was the analytical system used for the study. It provides numerous options for aerodynamic and structural modeling, which were exploited to determine the appropriate level of sophistication necessary for reliable rotor design optimization. There was a strong desire to tie the aeromechanics analyses to test data. The JVX rotor (Fig. 1) was chosen for the baseline because it is representative of the technology used in current tiltrotors (V-22 and BA-609). Moreover, its design and performance are well-documented in Refs. 7-8, which provide the basis for validation of the analytical methods used here (see also Ref. 4).



Fig. 1. The JVX rotor mounted on the PTR for hover tests at the OARF.

The CAMRAD II rotor model is described in the section Aeromechanics Analyses. The JVX rotor and its hover and high-speed (cruise) tests are described in the section JVX Test Rotor. The results of Ref. 4 are then summarized, along with discussions of the predictive methods employed. Having been validated, or at least calibrated, against test data, the aeromechanics analyses are then applied to variations of basic design parameters, notably solidity, taper, and twist, in the section Examples of Optimization. The section Additional Optimizations extends the analyses to sweep and droop. Although not emphasized, implications for the proprotor design itself are a natural fallout of the research and are summarized in the section Maximum Performance.

Aeromechanics Analyses

CAMRAD II is a comprehensive rotorcraft analysis code (Ref. 9), with a free wake model, a multi-element structural beam model, and a choice of stall delay models. It is much more computationally efficient than any equivalent CFD/CSD code. CAMRAD II is, therefore, ideally suited for determining the relative importance of different design parameters for performance. The latest CAMRAD II wake and stall-delay models were validated against the test data of Refs. 4 and 7. Every step of the procedure is thereby traceable to large-scale test data, albeit more directly for hover than for cruise.

Correlation with test data is presented in the section JVX Test Rotor. Five different levels of aerodynamic modeling

were evaluated: uniform inflow, differential momentum inflow (the CAMRAD II implementation of combined blade-element/momentum theory), prescribed wake (based on the Kocurek and Tangler model), free wake, and a multiple-trailer free wake (Ref. 10). In addition, two different, three-dimensional stall-delay models (Refs. 11 and 12) were evaluated, as were rigid and elastic blade models.

The rotor model had five elastic beam elements per blade (including the shank) with full hub and control-system kinematics. An axisymmetric solution (e.g., no gimbal motion) was used here, as appropriate for tiltrotor hover and cruise. The aerodynamic model also assumed axisymmetric flow. It had 31 aerodynamic panels per blade, more than would normally be needed, but useful for good definition of sweep and droop. Blade section properties were read from 2-D aerodynamic tables (Refs. 13 and 14). Rotating, 3-D stall delay was implemented as modifications to the 2-D aerodynamic table data, as discussed immediately below. Blade aerodynamics were modeled as a lifting line, optionally coupled to a wake model.

Stall-delay models

The following summary of the CAMRAD II stall-delay modeling options is adapted from Ref. 4. Proprotors are known to generate much more lift inboard than would be predicted from two-dimensional airfoil section data alone. The rotating blade experiences centrifugal pumping of the airflow, which accelerates the boundary layer and greatly delays stall, with the strongest effect at the root. CAMRAD II does not directly calculate this effect, but provides two different models for correcting 2-D airfoil data to account for 3-D stall delay. The dependence upon radius is specified separately and must be matched to the stall-delay model. Although this complicates the input, it provides for maximum flexibility in accommodating different rotor designs and stall-delay models.

The two stall-delay models are derived from Refs. 11 and 12. Examples of adjustments to 2-D properties for the familiar NACA 0012 airfoil are given in Fig. 2. Both models require empirical adjustments, but give equally good results for the JVX test data. In the absence of more computationally efficient CFD methods, this is the most practical method of incorporating stall-delay effects into design optimization.

The Corrigan model (Ref. 11) shifts the peak lift and stall recovery region upwards along a line defined by the lift-curve slope at zero c_l , extrapolated well beyond the normal stall angle. The extrapolated, linear lift curve is labeled “extended c_l ” in the figure. In contrast, the Selig

model (Ref. 12) is a weighted interpolation between the extended c_l and the airfoil table c_l , with a similar correction for c_d . In CAMRAD II, both stall-delay corrections are washed out angles of attack greater than 30 deg. The Selig model adjusts both lift and drag, but the Corrigan model adjusts only lift. The default stall-delay model for the JVX rotor is the Selig model, but both models were examined during the optimization studies.

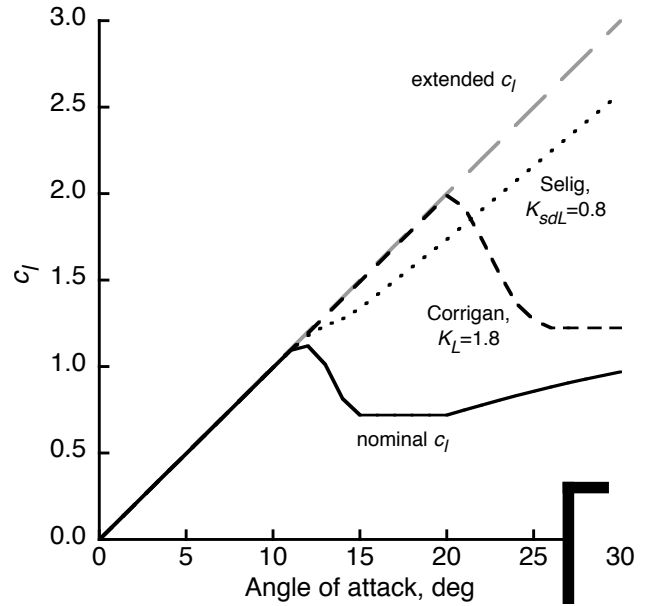


Fig. 2. 3-D stall delay models for the NACA 0012 airfoil.

For Corrigan stall delay,

$$c_l = K_L c_{l_{table}} \left(\frac{\alpha - \alpha_z}{K_L} + \alpha_z \right)$$

For Selig stall delay,

$$c_l = c_{l_{table}} + K_{sdL} (c_{l_L} - c_{l_{table}})$$

$$c_d = c_{d_{table}} + K_{sdD} (c_{d_L} - c_{d_{table}})$$

where

$$c_{l_L} = c_{l_\alpha} (\alpha - \alpha_z)$$

$$c_{d_L} = c_{d_z}$$

JVX Test Rotor

The following summary description of the JVX rotor and test history is adapted from Ref. 4; see also Refs. 7 and 8. The JVX rotor was an experimental precursor to the V-22 rotor. Sometimes referred to as a “2/3 scale V-22”, it in fact differed from the V-22 in several respects. Moreover, it was tested in two different aerodynamic configurations, so care must be taken when making comparisons with the production V-22 rotor and with other scaled V-22 rotors.

The JVX rotor was 25 feet in diameter, which is 0.658 scale referred to the original V-22 design. However, the production V-22 rotor was slightly enlarged for manufacturing reasons, so the JVX test rotor is more accurately 0.656-scale referred to the present V-22. The JVX rotor used an XV-15 hub with fixed, 2.5-deg precone, whereas the V-22 hub has a coning flexure with slightly different at-rest precone. An XV-15 spinner was used for JVX, instead of the much shorter V-22 spinner. JVX hover testing was done with the original taper and airfoil distribution, with linear taper and an XN-28 airfoil at the root. JVX high-speed testing was done with a thicker root section to better model the V-22 production blade. The JVX rotor was tested on the Propeller Test Rig (PTR), which has a fairing over the rotor balance just behind the hub (Fig. 1). The trailing edges at the JVX blade roots were slightly clipped to clear the balance fairing. All analyses reported here model the blade in the hover configuration, without the thicker root section. Nominal solidity (thrust-weighted) and taper are 0.1138 and 0.7, respectively, with a tip chord of 15.79 in.

The JVX rotor has spawned several progeny, all similar but none identical. JVX hover performance was better than expected due to stall-delay effects. The full-scale V-22 was subsequently built with slightly lower solidity than JVX and with a blade-fold hinge and fairing. The BA609 rotor is similar to JVX, but slightly larger in diameter and with a different root airfoil section (Ref. 15). There are also multiple small-scale aircraft, including TR911X and Eagle Eye, all using derivative rotors. None of these is an exact scaled version of JVX, and their differences must be kept in mind when comparing performance data.

JVX rotor tests

JVX hover tests were performed on the NASA Ames Research Center Outdoor Aerodynamic Rotor Facility (OARF) in 1984 (Ref. 7). High-speed (airplane-mode cruise) and wing download and interference tests were conducted in the 40- by 80-ft test section of the National Full-Scale Aerodynamics Complex (NFAC) at NASA Ames, divided into three test phases. Phase I tests were conducted in 1988. Only very limited cruise data from the Phase I test were collected and published (Ref. 8). The Phase II entry was in 1991 and generated a more comprehensive data set. The Phase II data were only recently published (Ref. 4). Phase III was intended to complete the high-speed data set, but the rotor was destroyed in an accident very early in the test.

The cruise data used for model validation and presented here are all from the surviving Phase II data set. Although the maximum speed attained was below the desired goal

of 300 knots, the data are adequate for the analytical comparisons included here.

Hover data

Hover test data are shown in Figs. 3 and 4 for average $V_{tip} = 754$ ft/sec, giving $M_{tip} = 0.676$. Data points were selected from those test conditions with a free-air wind speed of less than 1 knot. Figure 3 shows predictions made with a free-wake model, in which the shed vorticity is eventually rolled up into a single tip vortex (the rolled-up model). This is the default CAMRAD II free-wake model, with a strong vortex at the tip, a weak vortex at the root, and a vortex sheet in between. It gives good correlation with the OARF test data at high C_T , but underpredicts figure of merit at low C_T .

Predictions are also shown for a multiple-trailer model, which has an additional vortex trailer inboard of the radius at which blade-vortex interaction is experienced in hover (about 0.80 R). The multiple-trailer model fits the data better at low thrust than the rolled-up model (see Ref. 4 for further discussion). This is because the multiple-trailer model better accounts for blade-vortex interaction at low thrust, where the tip can be negatively loaded. The multiple-trailer model, however, requires much more computer run time than the rolled-up model, so the latter, simpler wake model is the default inflow model for all predictions presented here. The severe computational demands of the multiple-trailer model was an important motivation for the present research.

It should be noted that the multiple-trailer model used here is distinct from the CAMRAD II “dual-peak” wake model. The latter is intended for use with negative tip loading, whereas the former applies to both positive and negative tip loading.

Figure 3 also shows predictions made without any 3-D stall-delay corrections. Figure of merit is clearly underpredicted everywhere but very low thrust. The Selig and Corrigan stall delay models are difficult to distinguish at the scale of Fig. 3, the difference being barely one line thickness at most, so results for only the Selig model are shown.

Three additional, simpler aerodynamic models were also investigated. In increasing order of sophistication, they were uniform inflow, differential momentum theory (the CAMRAD II implementation of combined blade-element/momentum theory), and a prescribed wake model, here the Kocurek and Tangler model (Ref. 16). Figure 4 suggests that they all match the test data better than the rolled-up free wake model, but this is misleading. All three models rely upon empirical adjustments for good predictions of figure of merit.

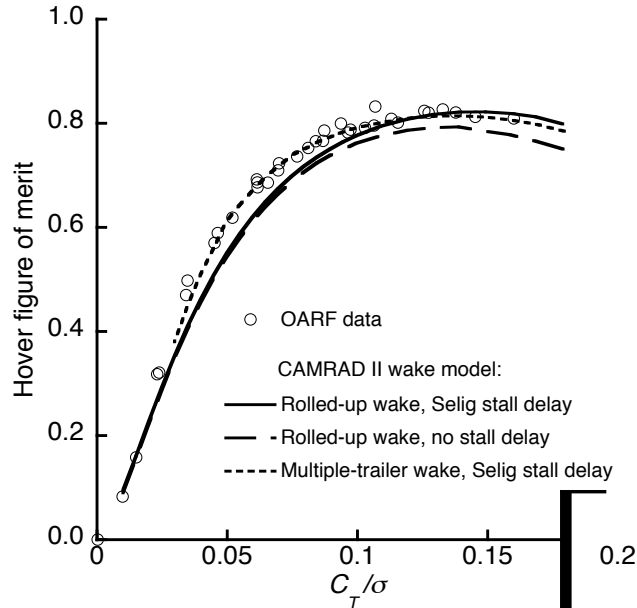


Fig. 3. JVX test data vs. CAMRAD II free-wake predictions of hover performance.

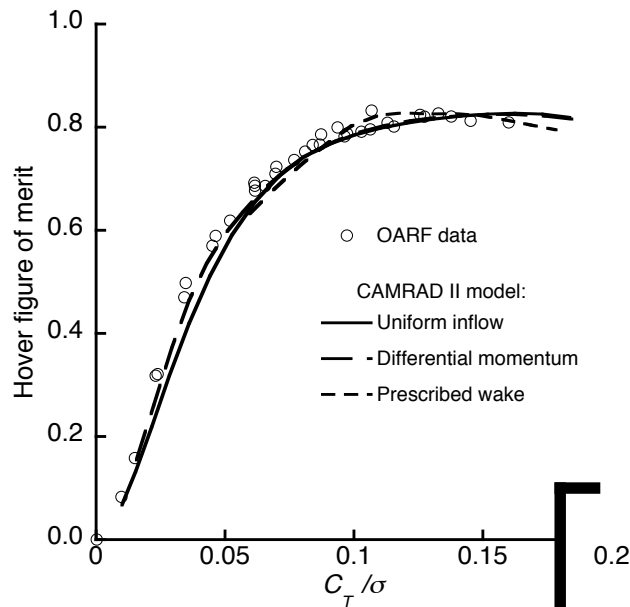


Fig. 4. JVX test data vs. CAMRAD II predictions of hover performance with simpler inflow models.

The uniform inflow and differential momentum models rely on an empirical factor on induced velocity, κ_λ , for a good fit to the data. To match the JVX hover data, $\kappa_\lambda = 1.10$ for uniform inflow, and $\kappa_\lambda = 1.04$ for differential momentum. Although these two models may give good fits to the hover data with appropriate values of κ_λ , they cannot be relied upon to give good performance estimates as blade design parameters are varied, because there is no way to determine in advance the correct values of κ_λ . Worse, these two models cannot possibly account for the

effects of wake distortion and vortex interactions. Nevertheless, the savings of computer resources motivated an examination of these models for rotor design optimization, where rapid narrowing of the design space may be more advantageous than exact predictions of performance.

Figure 4 also shows predictions made with the Kocurek and Tangler prescribed-wake model. Because of its simplicity compared to a free-wake model, the Kocurek and Tangler model would seem to be a candidate for performance analysis, but it too depends upon empirical adjustments, notably a factor on vertical convection. As with the uniform inflow and differential momentum models, the Kocurek and Tangler model was applied to rotor optimization in hopes of finding a more efficient solution than a free wake model.

Cruise data

The JVX airplane-mode data are plotted as power versus thrust in Fig. 5. Clustering into five groups of constant μ is obvious, as is the good fit of CAMRAD II predictions to the data. All data at $\mu = 0.523$ and below were taken at 487 rpm, but the data at $\mu = 0.562$ were taken at 531 rpm. (Propulsive efficiency η is the preferred parameter for optimization, but for this rotor, measurements of η at different advance ratios collapse on top of each other, making power the more useful parameter for validation.)

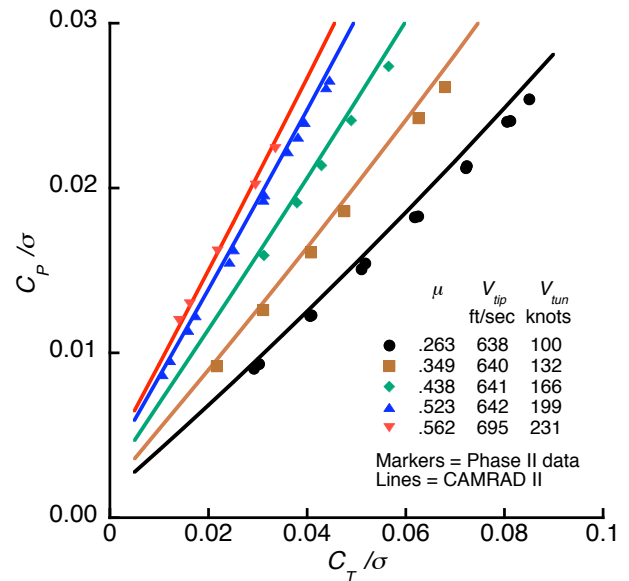


Fig. 5. CAMRAD II predictions of JVX cruise (airplane-mode) performance vs. test data.

The CAMRAD II predictions shown were made with the rolled-up free wake model. 3-D stall delay is not relevant at the low blade-lift coefficients typical of high speed, so

no stall delay model was used. The free wake, uniform inflow, differential momentum, and Kocurek and Tangler predictions are extremely difficult to distinguish from each other. The worst discrepancies are barely one line width at the scale of Fig. 5, so only predictions for the rolled-up model are shown. The multiple-trailer model was not used here, because blade-vortex interaction does not exist at high-speed axial flow, even at low thrust.

The predictions fit the data best at the highest speed, worst at the lowest, which is adequate for the optimizations presented herein. The reader is reminded that the excellent fit to the data by the less sophisticated models depends upon empirical adjustments to inflow velocity. To match the JVX cruise data, $\kappa_\lambda = 4.6$ for uniform inflow, and $\kappa_\lambda = 1.65$ for differential momentum.

Blade Design Parameters

The logic behind the choice and sequence of parameters analyzed deserves discussion. Rotor blade twist (and sweep, if utilized) has negligible effect on section structural properties. Minor changes to airfoils will also have minor effects on local structural properties, provided that thickness-to-chord ratio (t/c) is held constant. Conversely, substitution of new materials can have major effects on section mass and stiffness with no effect on aerodynamics. Hence, to first order, twist, sweep, airfoils, and materials can be adjusted independently of each other.

For sufficiently large changes in these parameters, there will be global changes in load distribution or blade deflection that couple aerodynamic and structural properties. For example, large tip sweep will introduce a torsion moment that will change the twist under load, with the amount determined by torsional stiffness. The significance of these effects can be determined by a comprehensive analysis such as CAMRAD II.

Another consideration for the present research is that modest variations in a few parameters, such as twist, sweep, taper and solidity, can be made without assuming any additional technology insertions. Optimization of these parameters best reveals the impact of new analytical methodologies, including free-wake and stall-delay models.

Other parameters, notably structural and airfoil properties, are more directly dependent upon new technology, and are also more open-ended. The design of blade structures and airfoils are major research areas in themselves, so the present effort includes only top-level estimates of structures and airfoil technology.

The JVX airfoils (Ref. 17) were designed for specified Mach numbers, so a rigorously fair examination of the effects of tip speed would require several new sets of airfoils, or at least different spanwise distributions of the existing airfoils. This would be a worthwhile research endeavor in its own right, but is outside the scope of the present effort.

To provide a consistent basis for comparison, key design parameters were held constant or limited to small variations, except in special cases. Rotor diameter and blade number are fundamental design choices. Diameter was always that of the JVX rotor (25 ft.). Blade number was kept at three, the same as the JVX rotor. Tip speed was held constant at 755 ft/sec (0.567 Mach) for hover (sea level standard conditions) and 643 ft/sec (0.676 Mach) for cruise (300 knots at 20,000 ft), both matched to the JVX airfoil nominal design conditions (Ref. 17). The actual JVX rotor design had to accommodate several additional operational criteria not addressed here; see Ref. 18 for details.

All calculations were performed at fixed values of hover and cruise thrust, derived from the design values of the JVX rotor: nominal hover $C_T/\sigma = 0.15$, and nominal cruise $C_T/\sigma = 0.056$. However, CAMRAD II was trimmed to thrust, not C_T/σ , because solidity was varied for some calculations. The results of these analyses will be used to support design studies, where aircraft gross weight, airframe drag, cruise speed and altitude, and other global design parameters will be derived from mission requirements by a sizing code. Thrust at a given airspeed and altitude is the appropriate trim condition, as appropriate for hover or cruise.

Examples of Optimizations

Examples of several different parameter optimizations are given here, for several different aeromechanics models. Solidity, taper, twist, sweep, and droop are all considered. Five different inflow models are applied: uniform inflow, differential momentum, prescribed wake (the Kocurek and Tangler model), free wake, and a multiple-trailer wake. Two different, three-dimensional stall-delay models were evaluated, as were rigid and elastic blade models.

Full optimization maps are usually presented, not just the envelopes. It is important that the results not be biased by a particular mission model, which may, for example, emphasize cruise performance more strongly than hover. It is also important to present sub-optimum design points and performance trends in order to reveal any deficiencies in the methodology. Full maps directly reveal the tradeoffs between cruise and hover performance, thereby

avoiding misleading conclusions that may arise from designing to a single mission specification.

Most optimization maps shown here include a design point representing the actual JVX rotor (in its original hover configuration), which establishes traceability back to test data. These criteria are relaxed in some of the plots, either to accommodate changes in scale or to summarize results of multiple optimizations.

The hover and cruise tests used different root airfoil sections, which makes it impossible to match all test configurations while keeping the aerodynamics consistent during hover and cruise optimizations. Using different airfoils for hover and cruise would be more problematic than a slight mismatch to the cruise test rotor, especially in view of the fact that the high-speed test data never fully matched the actual JVX cruise design conditions. Therefore, all analyses shown here are based upon the JVX hover configuration.

A major consideration in the choice of examples is the desire to clearly discriminate between different analytical methods. Accordingly, examples of poor predictions of performance trends or tradeoffs are presented along with the good, in order to identify and eliminate inadequate predictive models.

Rotor solidity is often determined early in the design process, because it determines maximum lift. For a fixed diameter, solidity and taper together determine blade chord, which is intimately connected to stall-delay effects. It is therefore appropriate to optimize solidity and taper together. Here, linear taper is used to allow direct comparison to the JVX test rotor.

Bilinear twist was developed for the XV-15 and is used on the V-22 and JVX rotors. It is a close approximation to the “ideal” twist derived from momentum theory (Ref. 19; see the Appendix for details). Note that this ideal twist is only an approximation, not only because of the limitations of momentum theory, but because a production rotor must compromise between different ideal distributions at different flight conditions. In any event, bilinear twist optimization proved a good method of distinguishing the effects of different aeromechanics models.

Droop and sweep have become increasingly common features of modern helicopter rotors, and have potential applications for proprotors. A few examples of droop and sweep are presented to illustrate where there is a clear failing of one of the aeromechanics models to properly capture the effect on performance.

Solidity and taper optimization

Figure 6 shows the effects of taper and solidity on performance as computed with the rolled-up free-wake model, plotted as figure of merit (FM) and propulsive efficiency (η); the baseline JVX test rotor is indicated by a black symbol. A 7x7 matrix of combinations of solidity and taper define the design space. Decreasing taper always improves η , but FM reaches a maximum at 0.8 taper (tip/root chord) and 0.11 solidity. Overall, hover performance is more sensitive to changes in taper and solidity than is cruise.

The optimum values of taper and solidity lie along the outer envelope of the optimization map; the exact optimum depends upon the mission specifications. This model—Selig stall delay, rolled-up wake, and elastic blades—is the reference model to which other variations will be compared.

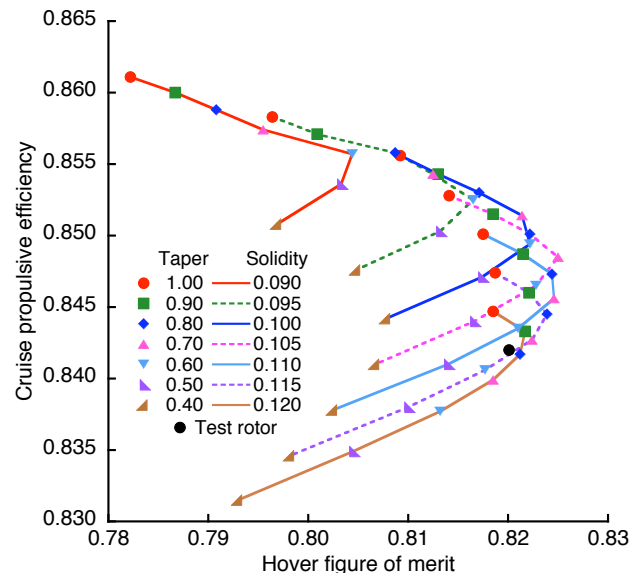


Fig. 6. Taper and solidity optimization for the JVX rotor with the rolled-up free wake model and the Selig stall delay model.

Figure 7 shows the taper/solidity map with the Corrigan model; the analysis is otherwise identical to that of Fig. 6. Comparing Figs. 6 and 7, the greatly expanded scales, relative to Figs. 3 and 4, reveal the difference in predicted figure of merit at the trim thrust. Figure 8 shows the results with no stall delay. These stall delay models affect hover only, so the values of propulsive efficiency are identical. The Selig and Corrigan models result in slightly different patterns and small changes in the optima. However, the results of using no stall delay are severely different from either model, both in the pattern and in the range of values of figure of merit.

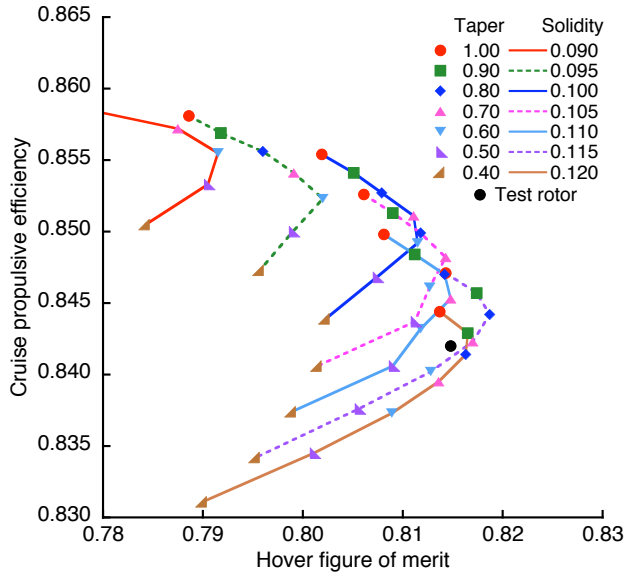


Fig. 7. Taper and solidity optimization with the Corrigan stall delay model (affects hover only).

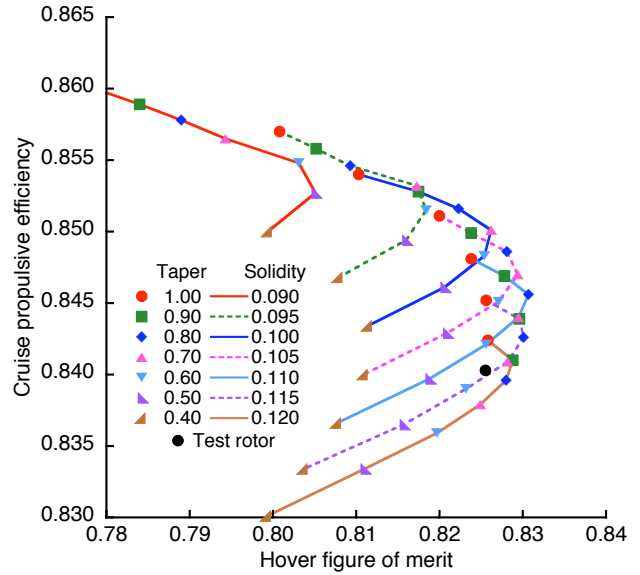


Fig. 9. Taper and solidity optimization with rigid blades and controls.

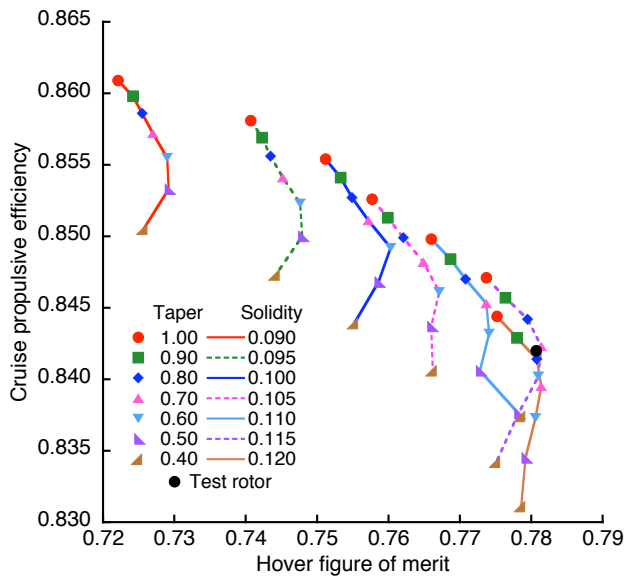


Fig. 8. Taper and solidity optimization with no stall delay model (affects hover only).

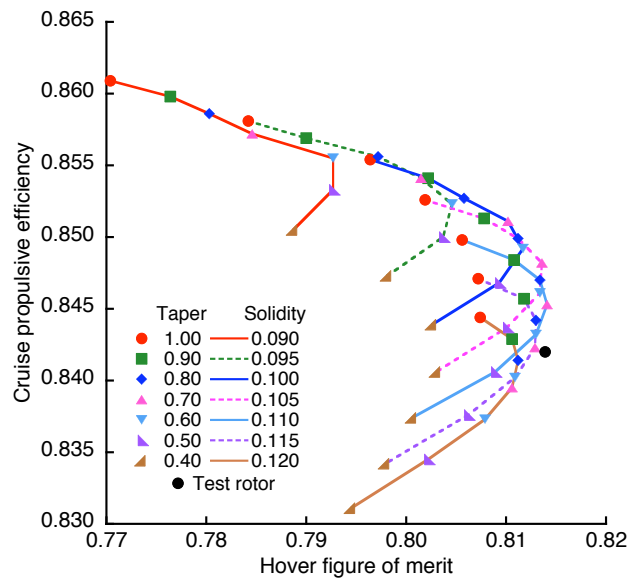


Fig. 10. Taper and solidity optimization with multiple-trailer wake model.

Figure 9 shows the results of using a rigid blade model combined with Selig stall delay. The pattern is nearly the same as that of the elastic-blade model (Fig. 6), but shifted to slightly higher values of figure of merit. This is reasonable because elastic coning should cause a slight reduction in thrust for a given torque.

Figure 10 shows the results of applying the multiple-trailer wake model, with Selig stall delay and elastic blades. The pattern is similar to that of the rolled-up model (Fig. 6), again with a slight shift in predicted performance for the baseline rot

Tentative conclusions are that a 3-D stall delay model is essential, but that either the Selig or Corrigan model is adequate. Neither an elastic blade model nor the multiple-trailer wake model is necessary. These results will be re-examined in the section Twist Optimization.

Turning now to simpler models, Figs. 11 and 12 show results for the uniform inflow and differential momentum models. Both models were empirically adjusted to match the hover data at $C_T/\sigma = 0.15$ (Fig. 4), to which the calculations in Figs. 6-12 were trimmed. For both models, the optimization maps are very poor, despite the excellent

match to the hover data for the calibrated baseline condition. There is no hope of an optimizer selecting the proper combination of solidity and taper.

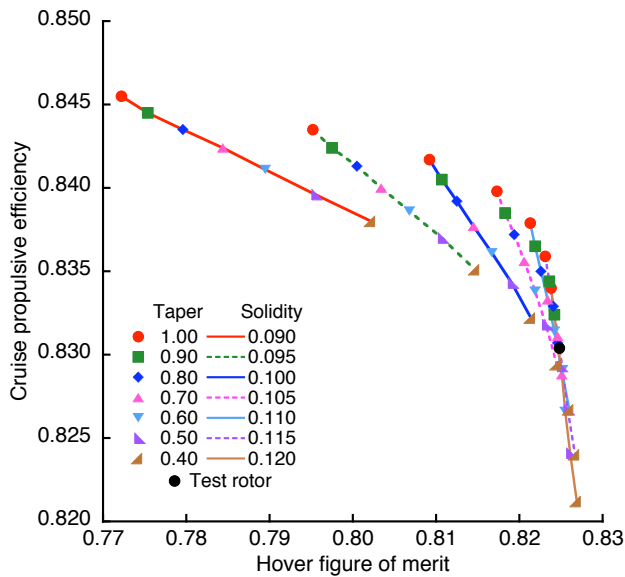


Fig. 11. Taper and solidity optimization with the uniform inflow model.

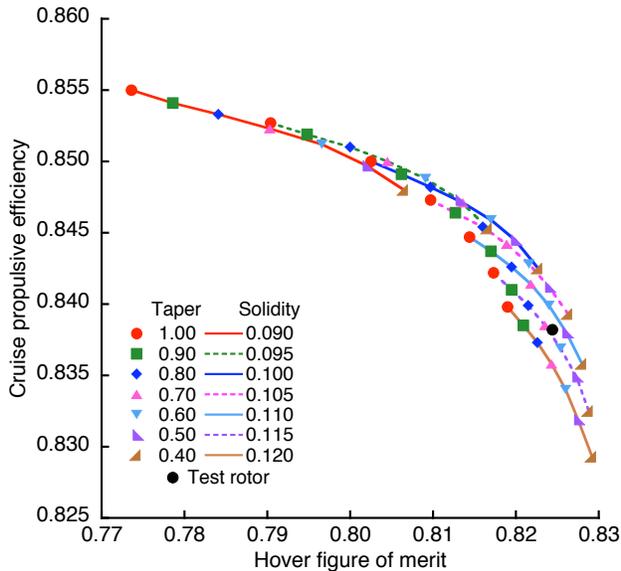


Fig. 12. Taper and solidity optimization with the differential momentum model.

The final model examined was the Kocurek and Tangler prescribed-wake model (Fig. 13). Again the map is extremely poor, and inadequate for a successful optimization. Although more sophisticated prescribed-wake models have been developed, all are potentially susceptible to the same problem: the wake geometry is indirectly dependent upon rotor characteristics that change as design parameters are varied. Unless the effects

of solidity and taper upon the wake geometry are known in advance and can be incorporated into the wake model, the effects upon rotor performance cannot be reliably captured.

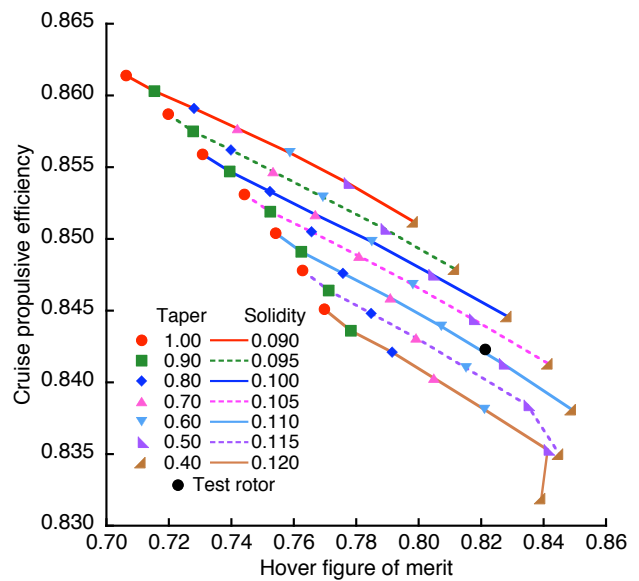


Fig. 13. Taper and solidity optimization with the Kocurek and Tangler prescribed-wake model.

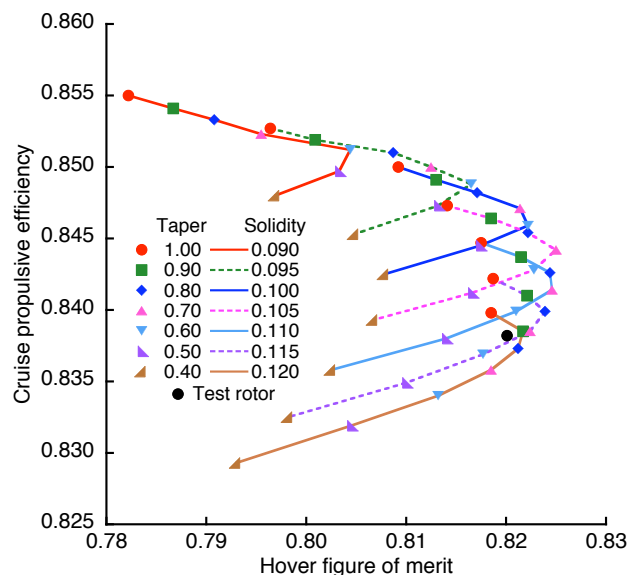


Fig. 14. Taper and solidity optimization with a mixed inflow model.

Although the differential momentum model gave poor results (Fig. 12), its predictions of propulsive efficiency are in fact nearly the same as the free-wake model of Fig. 6. Therefore, one could legitimately use the differential-momentum model in cruise and a free-wake model in hover. Fig. 14 shows the results of such a combination. The mixed inflow model generates the same pattern as Fig. 6, with a slight overall reduction in propulsive

efficiency, but the optimum combinations of solidity and taper along the outer envelope are the same.

Twist optimization

The same CAMRAD II rotor and inflow models used for solidity and taper optimization were applied to twist optimization. Bilinear twist applies a constant twist rate from the blade root to a given transition radius, then a different rate to the tip. For the examples shown here, the transition radius was $0.45 R$, which is a close match to the JVX test rotor (the twist distribution of the actual rotor is blended in the vicinity of $0.45 R$, whereas the distributions studied here are exactly bilinear). Twist is here always indexed with zero twist at $0.75 R$.

Figure 15 shows a conventional twist optimization map for combinations of inboard and outboard linear twist, all using the rolled-up wake model with Selig stall delay. A large matrix (7×7) of combinations of inboard and outboard twist rates was analyzed to map out the design space. Cruise conditions favor lower inboard twist and higher outboard twist than does hover. FM tends to be more sensitive to outboard twist rate, while η is more sensitive to inboard twist. For the twist variations examined here, the ranges of variation of FM and η were somewhat greater than those for solidity and taper variations (compare Figs. 6 and 15). There are fewer practical design constraints upon blade twist than upon planform, so twist was varied more freely than solidity or taper.

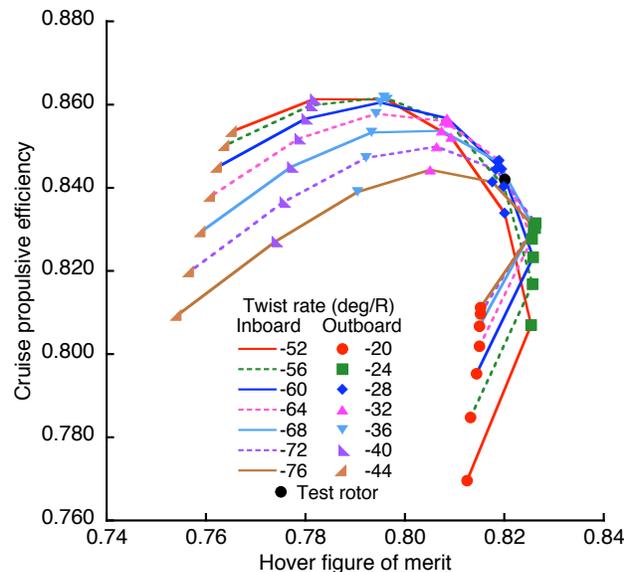


Fig. 15. Bilinear twist optimization for the JVX rotor with the rolled-up free-wake model and the Selig stall-delay model.

The twist map with the Corrigan stall delay model (Fig. 16) is closely similar to that for Selig stall delay, although figure of merit is reduced at off-optimum values of twist. With no stall delay model (Fig. 17), the outer envelope of the twist map is superficially similar to those for the two stall delay models, but the optimum values of twist are incorrect for hover. The effect of inboard twist rate is not properly captured, which is not surprising because stall delay applies much more strongly inboard than outboard. The results near peak cruise performance are similar for all of Figs. 15-17, simply because 3-D stall delay does not apply in cruise.

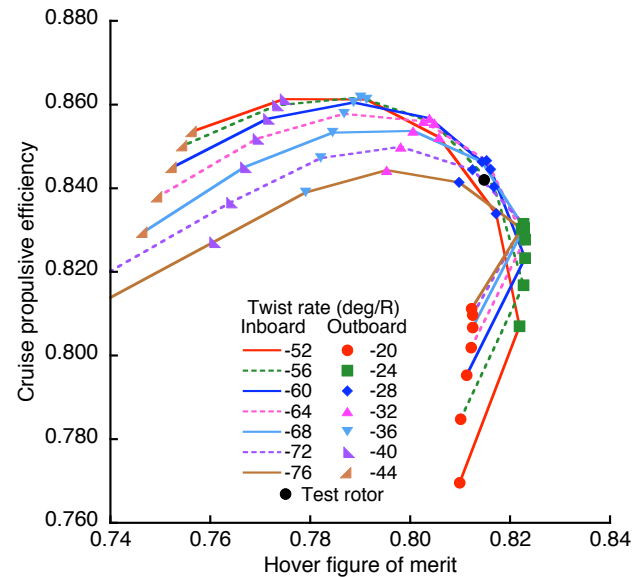


Fig. 16. Bilinear twist optimization for the JVX rotor with the Corrigan stall-delay model (affects hover only).

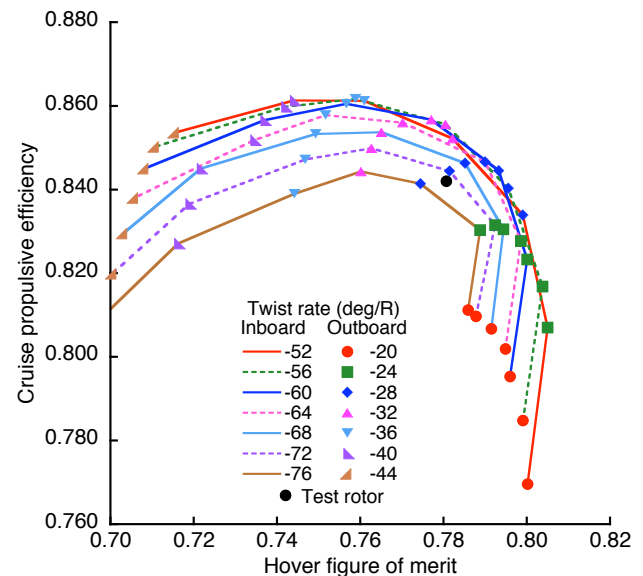


Fig. 17. Bilinear twist optimization for the JVX rotor with no stall-delay model (affects hover only).

Results for the rigid blade model are shown in Fig. 18, and for the multiple-trailer wake model in Fig. 19. The structural model makes little difference (compare Figs. 15 and 18), except at certain extreme values of twist. The multiple-trailer model yields a smaller range of variation in figure of merit than the rolled-up model (compared Fig. 15 and 19), but the parameter values along the outer envelopes of the optimization maps are almost the same.

These results for twist are consistent with those for solidity and taper: a 3-D stall delay model is necessary, but either model (Selig or Corrigan) is adequate, and an

elastic blade model is unnecessary, as is the multiple-trailer wake model.

Results for the uniform inflow model and the differential momentum model are shown in Figs. 20 and 21. The patterns are similar. Neither model properly captures the effect of inboard twist anywhere, nor of outboard twist near peak propulsive efficiency. The effect of outboard twist near peak figure of merit is approximately calculated, but this is not enough to guarantee that an optimizer will find the correct combination of inboard and outboard twist.

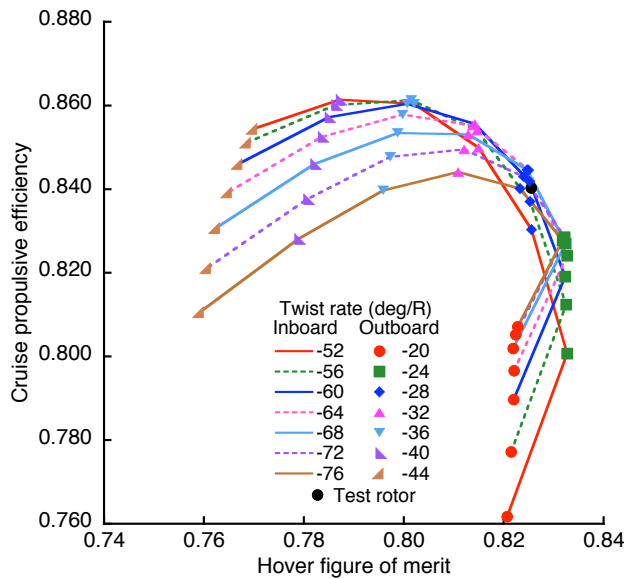


Fig. 18. Bilinear twist optimization for the JVX rotor with rigid blades.

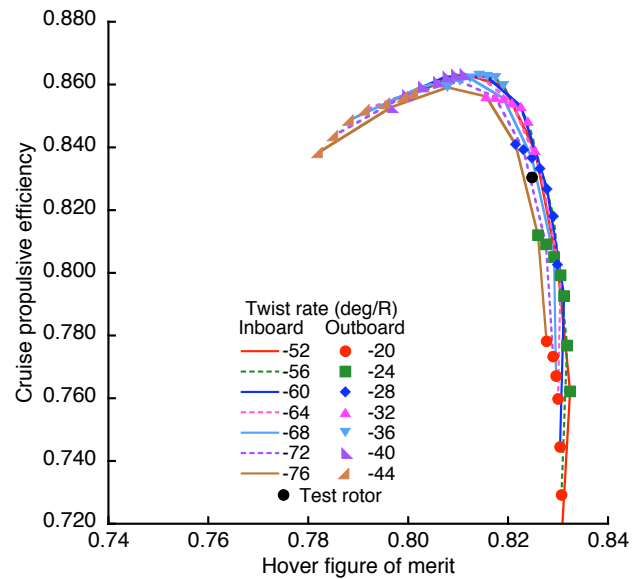


Fig. 20. Bilinear twist optimization for the JVX rotor with the uniform inflow model.

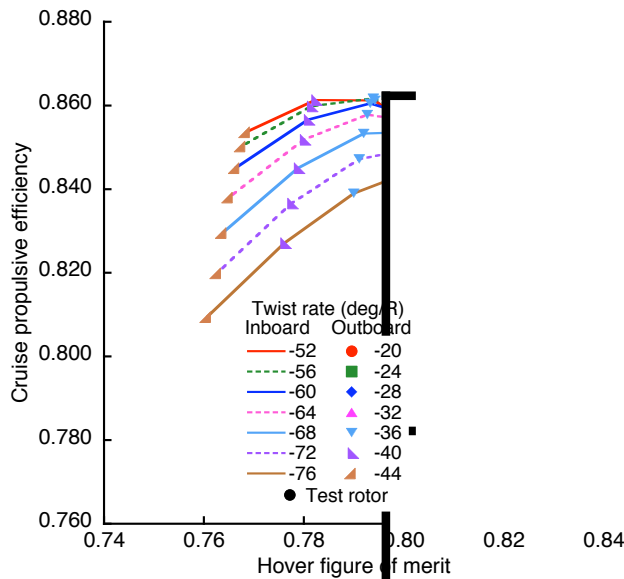


Fig. 19. Bilinear twist optimization for the JVX rotor with the multiple-trailer wake model (affects hover only).

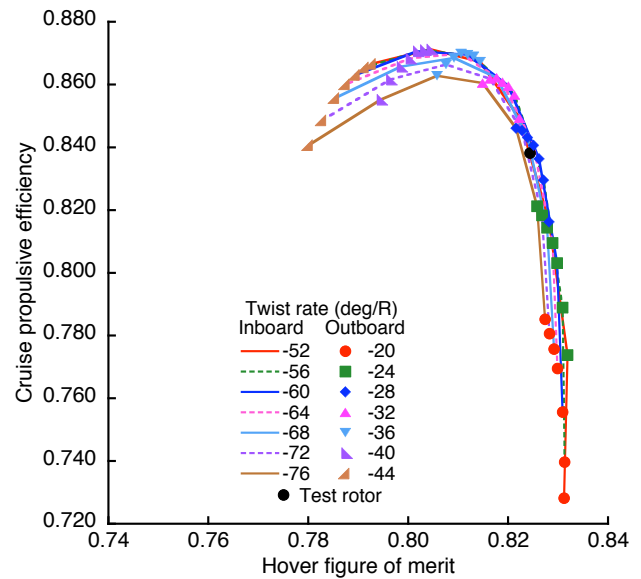


Fig. 21. Bilinear twist optimization for the JVX rotor with the differential-momentum inflow model.

Figure 22 shows results for the Kocurek and Tangler prescribed wake model. Although the outer envelope appears similar to that for either free wake model, the effect of outboard twist on the peak value of figure of merit is poorly represented. This is despite adjustment of the prescribed wake geometry to match the variations in outer blade twist. As with the uniform inflow and differential momentum models, the prescribed wake model would not lead an optimizer to the correct design values of twist, except perhaps for a rotor designed strictly for maximum cruise performance.

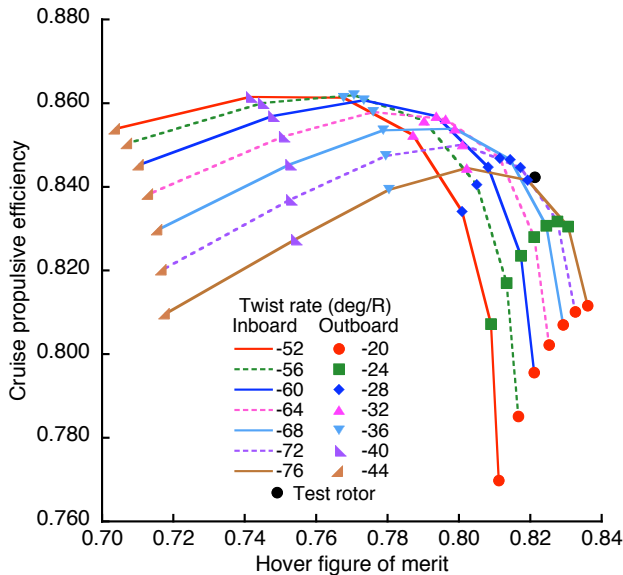


Fig. 22. Bilinear twist optimization for the JVX rotor with the prescribed-wake model.

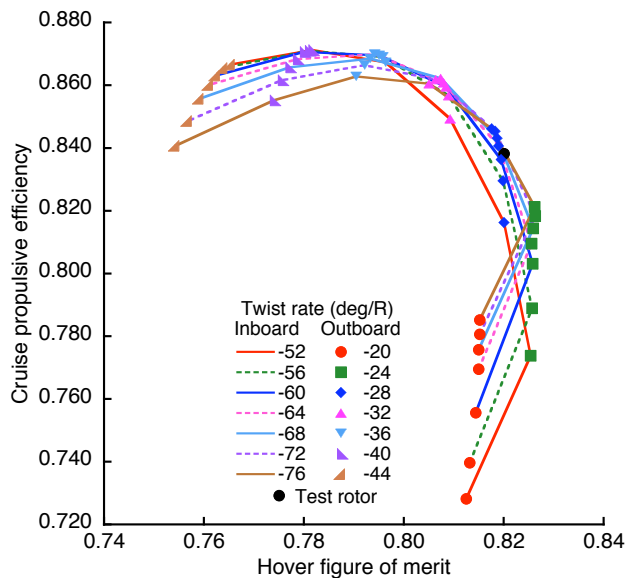


Fig. 23. Bilinear twist optimization for the JVX rotor with a mixed inflow model.

A mixed inflow model, using differential-momentum inflow in cruise and a rolled-up free wake in hover, is used to generate the twist map in Fig. 23. Compared to the full free-wake model (Fig. 15), it is less sensitive to inboard twist near peak propulsive efficiency, but more sensitive near peak figure of merit. However, the greatest differences are for non-optimum values of twist. The optimum values of twist along the boundaries of the twist maps are nearly the same.

Preliminary conclusions Based upon the results for solidity, taper, and twist optimization, a few conclusions may now be drawn concerning the analytical models. The criterion for proper optimization is that the model must indicate the correct values of the design parameters, not that figure of merit and propulsive efficiency be perfectly predicted.

The two stall delay models were equally good for optimization. The Selig model was chosen for all further studies, largely for convenience. (The pattern for solidity/taper optimization was a little more consistent than that for the Corrigan model, but this may be an artifact of the CAMRAD II trim strategy.) Optimizations without any stall delay model were clearly poor and were not further considered.

The structural model also made little difference. The rigid model is here preferred for further studies of the JVX rotor because of its simplicity. However, this choice may not be appropriate for other rotors: the JVX rotor is much stiffer than many helicopter rotors, and new proprotor concepts (e.g., those of Ref. 1) with different dynamic characteristics may require an elastic structural model.

The Kocurek and Tangler prescribed wake model is inadequate for determining the optimum values of solidity, taper or twist. While it is conceivable that a more refined prescribed-wake model might provide reasonable estimates, there is very little savings in computational time compared to the rolled-up wake model. There is, therefore, no practical advantage in using the Kocurek and Tangler model.

Although the multiple-trailer wake model is theoretically more accurate than the rolled-up model, there are negligible differences in the optimal values of solidity, taper, or twist. More critically, the multiple-trailer model requires vastly more computational time than the rolled-up model, and is for that reason alone not recommended for routine optimization.

The mixed-inflow model—differential momentum in cruise and rolled-up wake in hover—yields very nearly the same results as using the rolled-up wake model

exclusively. Where saving computational time is critical, this model may be an acceptable compromise.

Alternative twist distributions Before leaving the subject of twist, it is worthwhile examining the effect of transition radius. Although not a formal part of the present research, a few interesting results could be immediately derived from the optimization studies.

Fig. 24 shows the envelope of several twist maps, each for bilinear twist but with different transition radii. Note that Figs. 15-23 collapse four variables—inboard and outboard twist rate, figure of merit, and propulsive efficiency—into two dimensions. By suppressing the details of the underlying optimization maps, Fig. 24 adds a fifth parameter, namely transition radius. The exact transition radius makes negligible difference near peak propulsive efficiency, where there is less difference between the inboard and outboard twist rates than at maximum figure of merit. There is little to choose between the $0.45-R$ and $0.50-R$ transition radii; the first is perhaps slightly better and more closely matches the actual JVX twist distribution, so it was the preferred value for all other results presented here.

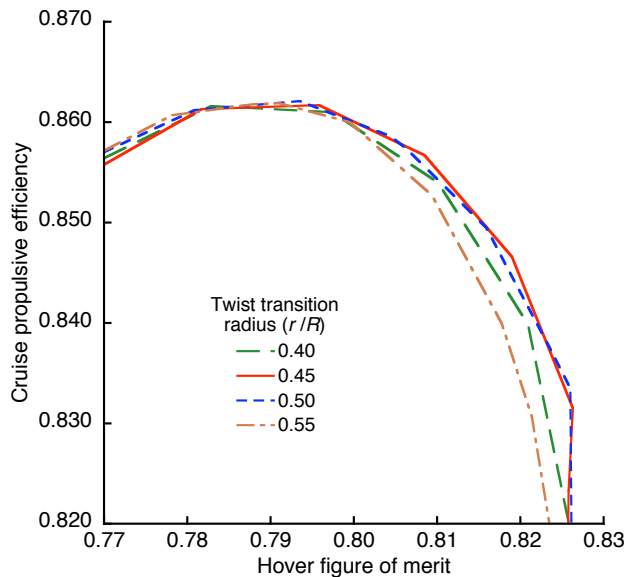


Fig. 24. Bilinear twist envelopes with different transition radii.

Figure 25 replots the envelope for the $0.45-R$ transition radius against ideal twist. Applying the method of Ref. 19, ideal twist was determined separately for hover and cruise (see also the Appendix). Weighted averages of the hover and cruise distributions were calculated, then the twist of each weighted distribution was scaled up or down by varying percentages of total twist. The hover/cruise weighting factor and the total-twist scaling factor com-

prised the optimization parameters for ideal twist. The boundary of the resulting twist map is plotted in Fig. 25.

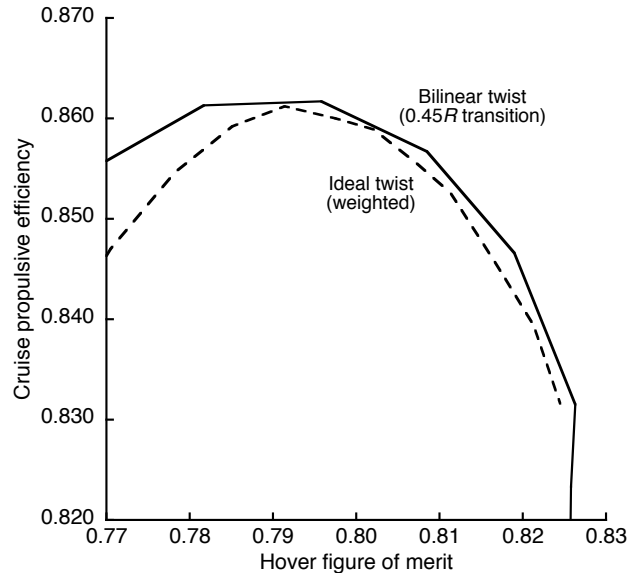


Fig. 25. Optimization envelopes for bilinear twist and ideal twist (weighted).

The ideal twist distribution, even when weighted and scaled, does not provide quite as good performance as the best bilinear distributions. Given that ideal twist is derived without full consideration of wake effects, it is not surprising that it falls slightly short. Indeed, the results are perhaps better than might be expected.

Additional Optimizations

Several additional design parameters were analyzed, but not all of them proved to be significantly affected by the choice of analytical model. In particular, variations in airfoils were not good discriminators between the models. Changes in maximum section lift capability affected mostly hover performance, while changes in sensitivity to Mach number affected mostly cruise. Drag reductions were beneficial everywhere. However, the results varied little between inflow models, with negligible effect upon the optimum values. The results for airfoils were thus unremarkable and are accordingly not shown here.

In contrast, variations in droop and sweep yield drastically different results for different inflow models, and so merit discussion. Some subtleties in the definitions of droop and sweep used here should be mentioned. In the basic definition, both droop and sweep are initiated at a transition radius r_{ds} , respectively perpendicular or parallel to the rotor plane (Fig. 26). For droop, the total blade area increases by an inverse cosine factor. However, neither the projected blade area nor the radius changes for pure

droop, but projected radius increases for sweep. It is not geometrically possible to simultaneously maintain all applicable parameters—total radius, droop/sweep transition radius, blade chord, disk area, and solidity—at identical, constant values for both droop and sweep while varying these two parameters. The approach used here fixed R at the nominal value for the unmodified blade, and allowed the blade area and projected radius R' to change as dictated by the specified values of r_{ds} and the droop/sweep angle.

An additional complication is that the combination of high blade twist and the large change in collective pitch between hover and cruise makes it impossible to have pure droop or sweep at all blade radii and at all trimmed flight conditions. Because droop is mostly beneficial to hover, droop is here applied perpendicular to the rotor plane when the unmodified blade is trimmed in hover. At high collective pitch angles in cruise, effective droop is reduced and there is an unavoidable component of forward sweep at the tip.

Sweep is beneficial to both hover and cruise, and so is applied in the rotor plane with the rotor trimmed to zero collective. Sweep is, therefore, nearly in-plane to the local chord from $0.75 R$ to the tip. In hover, there is a slight component of droop, and a larger amount of droop in cruise. This avoids negative droop (dihedral) at any trimmed flight condition.

An additional refinement over simple sweep, as in defined Fig. 26, is to implement sweep with a parabolic radial distribution. This has several advantages. A parabolic

distribution, with the sweep angle varying as $(r-r_{ds})^2$, is a close approximation to aerodynamically ideal sweep, wherein the effective local chordwise Mach number is constrained to some fixed value along the swept section. Parabolic sweep is here defined by the maximum sweep angle, at the tip. Parabolic sweep more smoothly blends the swept section with the inboard blade than either ideal sweep or simple sweep. This avoids a kink and resulting concentrated loads at r_{ds} . For CAMRAD II analyses, parabolic sweep replaces a single large angle in the lifting line with a series of more shallow angles along the swept section. This reduces numerical problems in the aerodynamic solution.

The effects of droop and sweep are shown here only for the rigid blade model. Droop moves the blade center of gravity perpendicular to the rotor plane, which changes elastic coning. Because an actual test rotor would probably use a different precone angle to compensate, an elastic blade model would make it impossible to separate the inertial and aerodynamic effects. Blade sweep moves the tip center of pressure aft of both the inboard elastic axis and the pitch axis, which twists the blade under load, usually unfavorably. A test rotor could compensate for this with a different twist distribution. For the present research, a rigorous twist reoptimization at each sweep configuration would require a four-parameter optimization, which again makes it difficult to separate the effects of different parameters (sweep angle, r_{ds} , and twist). Although not perfectly rigorous, a rigid blade model makes it possible to analytically decouple these effects, which is appropriate for the present research.

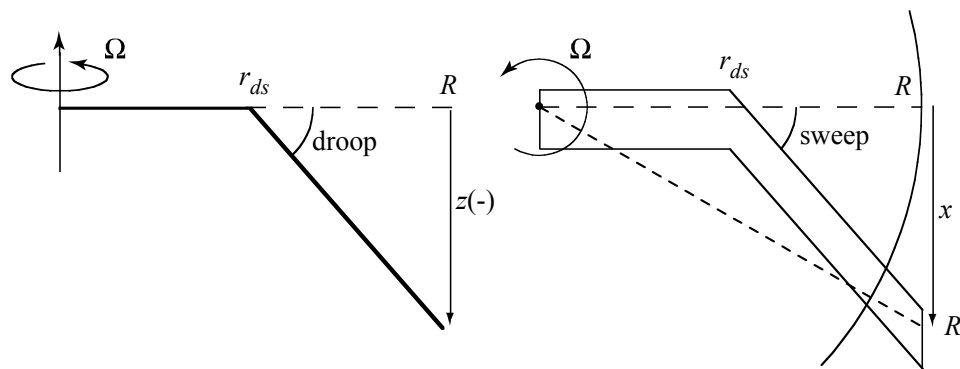


Fig. 26. CAMRAD II droop and sweep geometry (angles and offsets exaggerated).

Droop

Figure 27 shows results for several combinations of droop angle and transition radius (r_{ds}), here for the rolled-up free-wake model and Selig stall delay (the default aerodynamic model) and rigid blades. Increasing the length of the drooped section (decreasing r_{ds}) at a given droop angle improves propulsive efficiency up to about $0.85 R$, but has little effect thereafter. Increasing the droop angle always benefits figure of merit, more so at the largest transition radius than the lowest. For the most effective combinations of droop angle and transition radius, figure of merit is improved roughly twice as much as is propulsive efficiency. This is reasonable, given that droop is defined for the trimmed hover condition.

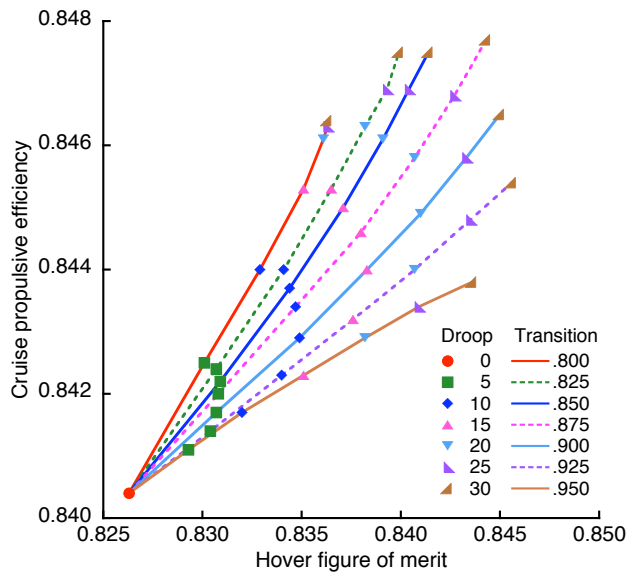


Fig. 27. JVX tip droop optimization with the rolled-up free wake model.

The same combinations of droop angle and transition radius shown in Fig. 27 were analyzed with the differential-momentum inflow model (Fig. 28). The effect on figure of merit is seriously incorrect, which is to be expected because droop improves hover performance by displacing the tip vortex. Without a tip vortex model—that is, a wake model—this effect cannot possibly be calculated correctly. However, a mixed-inflow model, with the rolled-up free wake model in hover and the differential-momentum model in cruise, gave results nearly identical to Fig. 27 (hence are not shown).

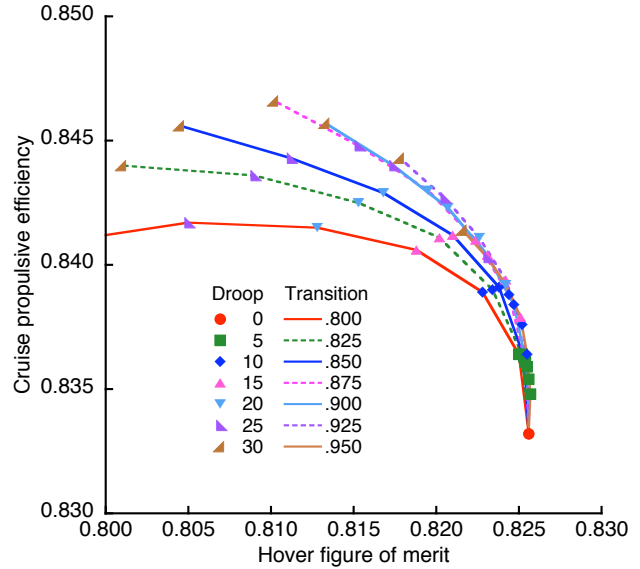


Fig. 28. JVX tip droop optimization with the differential-momentum inflow model.

Sweep

Results for several combinations of tip sweep angle and transition radius are shown in Fig. 29. Parabolic sweep is used; the sweep angles given in the figure are those at the tip. Sweep is here limited to 15 deg, for two reasons: large amounts of sweep reduce wing/rotor clearance in cruise, and are therefore impractical; and too much sweep and accompanying in-plane offset of the lifting line gives numerically invalid results. Nevertheless, it is clear that sweep improves figure of merit much more so than propulsive efficiency. Propulsive efficiency is sensitive to the effective Mach number at the tip, which is reduced by sweep, while figure of merit benefits both from the reduced Mach number and the displacement of the tip vortex. With an elastic blade model, the results show slightly less effect of transition radius, but are otherwise nearly the same as Fig. 28 (hence are not shown).

Two important qualifications apply to the results for sweep. Sweep reduces the local lift-curve slope, so that the twist over the swept section may no longer be optimum. It was not the purpose of the present research to define the best possible rotor, so a complete twist reoptimization was not performed for each sweep/radius combination. Further improvements in performance are therefore possible; simple examples are given in the section Maximum Performance. The second qualification is that the swept lifting line encountered numerical problems at large values of sweep. There could easily be numerical errors at the values shown in Fig. 29, so the results are overly optimistic for figure of merit.

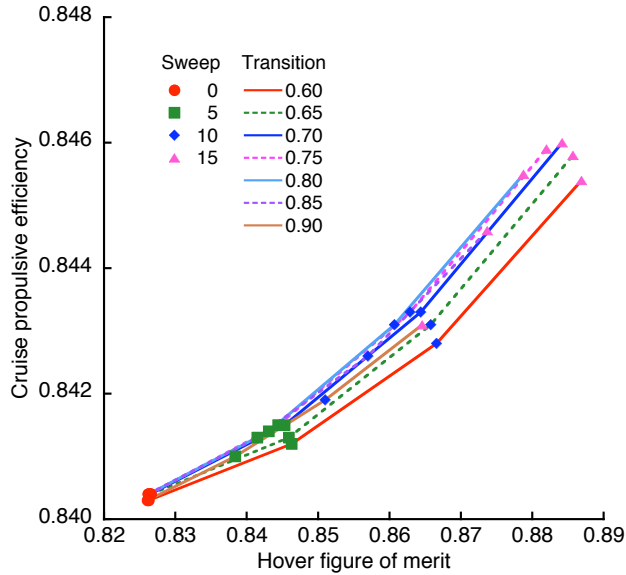


Fig. 29. JVX tip sweep optimization with the rolled-up free wake model.

The same combinations of sweep and transition radius shown in Fig. 29 were analyzed with the differential-momentum inflow model; the results are shown in Fig. 30. It is immediately evident that the simpler model cannot correctly predict the effects of sweep on hover performance.

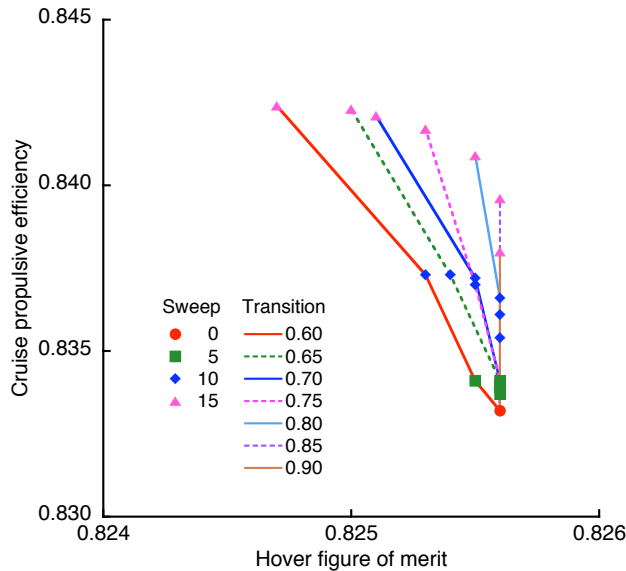


Fig. 30. JVX tip sweep optimization with the differential-momentum inflow model.

Because of the reduction in wing/rotor clearance, the swept blades of Figs. 29 and 30 are impractical, or at least would require a longer rotor shaft or other design changes. Results for an alternative implementation of sweep are shown in Figs. 31 and 32. Here, parabolic

sweep is applied to the leading edge only, so as to maintain a straight trailing edge. This requires the blade to be parabolically tapered; the resulting planform looks much like a modern, high-speed propeller. The blade chord was uniformly scaled to maintain constant solidity for all combinations of sweep and transition radius.

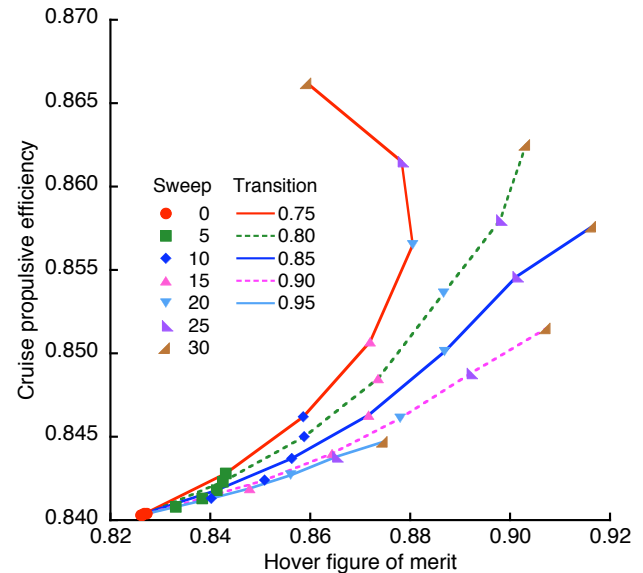


Fig. 31. JVX tip sweep optimization with no trailing-edge sweep and the rolled-up free wake model.

With the rolled-up wake model, parabolic sweep with a straight trailing edge provides large benefits to both cruise and hover performance (Fig. 31). Increasing sweep and transition radius always benefit propulsive efficiency, which should be expected to benefit from both the reduced chord and the reduced effective Mach number over the swept section. Figure of merit also benefits, but if the swept section is too large (the transition radius is too far inboard), hover performance is adversely affected. This effect is at least partly due to non-optimum twist. The same caveats discussed for Fig. 29 also apply here: the improvements to figure of merit are overly optimistic.

As a check on the numerical issues associated with a swept lifting line, the optimization of Fig. 31 was run with a straight lifting line (Fig. 32). This model is equivalent to a parabolically tapered tip with Mach relief applied to the airfoil coefficients, but with no geometric sweep. The benefits to η of Mach relief and taper are still seen, but not the effects of displacement of the tip vortex on FM.

Also shown in Fig. 32 is the optimization for pure parabolic taper: the same variations in planform as the other curves in the figure, but with no sweep. The curves for different transition radii collapse on each other, so only the outer envelope is shown. Tip taper is responsible for slightly less than half of the gain in η . If the sweep

optimization is run with only Mach relief, but no taper or lifting-line sweep, the results collapse into a vertical line almost identical to that for 0.90 transition radius. Hence, taper and Mach relief each contribute about half of the performance gain in cruise.

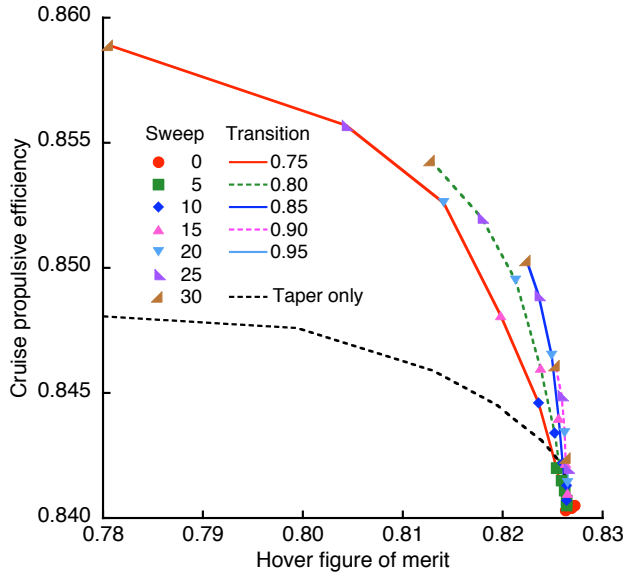


Fig. 32. JVX tip sweep optimization with no trailing-edge or lifting-line sweep and the rolled-up free wake mode

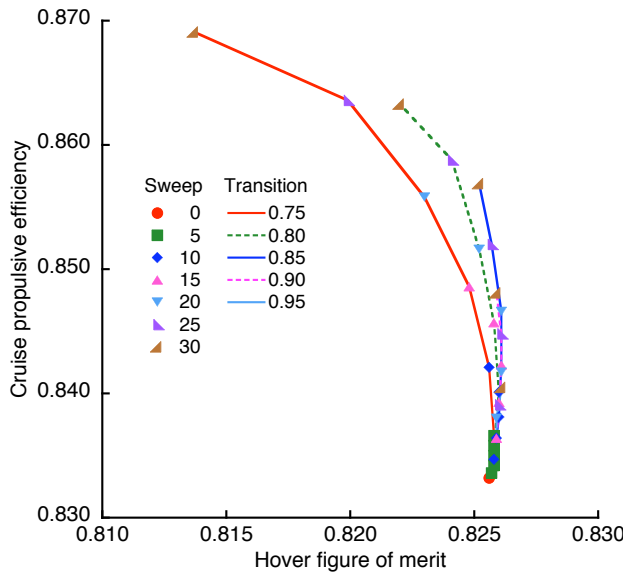


Fig. 33. JVX tip sweep optimization (straight trailing edge) with the differential-momentum inflow model.

The differential-momentum model was applied to the same combinations of sweep and transition radius shown in Fig. 29 for a straight trailing edge; the results are shown in Fig. 33. The pattern is similar to that for a straight lifting line (Fig. 32), but expanded vertically in

scale. Again, the simpler model cannot correctly predict the effects of sweep on hover performance.

Taken together, the results of Figs. 31 and 32 suggest that, even if CAMRAD II overestimates the improvement to FM, a swept and tapered tip can yield important performance benefits for a proprotor. At worst, a small amount of sweep and accompanying taper ($r_{ds} \leq 0.85 R$ in Fig. 32) can improve η by roughly 0.1 with negligible reduction in FM. At best, there is a very large potential improve also to be had in FM, but determination of the exact amount will require a more sophisticated analysis than CAMRAD II.

Maximum Performance

The best rotor design cannot be defined without a proper mission model. It was not the purpose of this research to derive such a model, but some simple criteria can yield estimates for the potential performance gains achievable with the methods developed above. The criteria were simply to maximize FM and η for hover or cruise respectively, with the constraint that neither could fall below 0.80 while maximizing the other (this constraint was based on the JVX rotor performance goals given in Ref. 18).

Taper and solidity were chosen first from Fig. 6, then twist (bilinear) was reoptimized. This yielded two rotor designs, optimized exclusively for hover or cruise. The improvements to FM and η , relative to the baseline JVX rotor, are tabulated in Table 1. For example, the improvement to figure of merit for the hover-optimized rotor is +0.004, under “Max Hover.” The process was repeated for the swept-tip rotor (parabolic sweep, straight trailing edge). Those results are summarized in Table 1 on the row labeled “Best sweep.”

Table 1. Maximum optimized performance improvements for hover or cruise.

Optimization	Max Hover	Max Cruise
Best taper and σ	$\Delta FM = +.004$	$\Delta \eta = +.034$
Best sweep	$\Delta FM = +.097$	$\Delta \eta = +.033$

Very little improvement should be expected for maximum hover performance when optimizing taper, solidity, and sweep, simply because the JVX test rotor was already optimized to similar criteria (Ref. 18), although with different methods than used here. When optimizing for tip sweep, however, hover performance improves dramatically. Even if the CAMRAD II predictions are highly exaggerated, there is still a potentially significant gain. Maximum cruise performance is about the same for either

optimization, although other performance criteria (e.g. low-speed maneuvering) would limit the gain for a practical rotor.

Conclusions and Recommendations

The purpose of this study was to determine the level of aeromechanics analysis necessary for successful proprotor design optimization, with emphasis on aerodynamics. All analyses were performed with CAMRAD II and were constructed so as to be traceable to experimental data for the JVX rotor. Propulsive efficiency and figure of merit were simultaneously optimized. The best tradeoff between predictive accuracy and computational efficiency was found to be a conventional free wake model, although a mixed-inflow model using a free wake in hover and differential momentum inflow in cruise (here, 300 knots at 20,000 ft) may often be appropriate.

Although a multiple-trailer wake model gave a more accurate fit to the test data compared to the conventional rolled-up vortex model, its use made little difference in the optimum values of solidity, taper or twist. Critically, the severe computational demands of the multiple-trailer model made it impractical for routine use.

Careful attention must be paid to the robustness of the aerodynamic analyses underlying any design optimization. Two analytical methods—differential momentum inflow and multiple-trailer free wake—both gave excellent fits to the best available test data, and their performance predictions were nearly indistinguishable from each other for the baseline rotor. Yet the optimization results were greatly different. A prescribed wake model (the Kocurek and Tangler model) also gave a good fit to the test data near the design thrust, yet it completely failed to capture the performance trends during the optimization of solidity and taper, nor of twist in hover. Physical considerations imply that computation of the self-distortion in a free-wake model is necessary to properly analyze even minor design changes, at least in hover.

While it was hoped that one or more of the simpler methods might be useful for design optimization, perhaps by scaling or otherwise adjusting the resulting optimization maps, there was no evidence that such can be achieved. The one exception was that a differential momentum solution (the CAMRAD II implementation of combined blade-element/momentum theory) gave good results in cruise, where free-wake effects do not dominate the flow as they do in hover.

The use of a 3-D stall delay model proved essential. Either of two stall delay models, the Corrigan and Selig models, gave nearly equivalent results. On the other hand, an elastic blade model was unnecessary, but this may apply only to proprotors similar to the JVX, which is much stiffer than conventional helicopter rotors.

In the absence of experimental test data for any of the designs generated during this study, these conclusions are, strictly speaking, based upon considerations of consistency, not absolute accuracy. Failure to exactly match test data, or to track performance as the design is varied, would be acceptable as long as the correct values of the design parameters are chosen by the optimizer. Even a failure to settle on the exact optimum would be acceptable if there were a major savings in computer time; a more accurate analysis could then be applied to a reduced design space. However, this would require trends in performance to be reasonably approximated, which was not the case in hover for any method less sophisticated than a rolled-up free wake with 3-D stall delay.

The study was extended to examinations of tip droop and sweep. The most significant results were perhaps those for parabolic leading-edge sweep at the tip, wherein enough taper was applied to keep the trailing edge straight. This was to maintain wing-rotor clearance at the nominal value in cruise. Large improvements in both cruise and hover performance were achieved. However, CAMRAD II relies upon a lifting-line analysis for blade aerodynamics, which is susceptible to numerical problems with a swept blade. Also, CAMRAD II does not have a fine-scale model for the formation of the tip vortex: its location and core size are fixed. Any blade modification that affects the formation of the tip vortex, or the circulation distribution near the tip, can potentially lead to an inaccurate tip-vortex model; this specifically includes droop and sweep. Nevertheless, the benefits of drooped and swept tips are well established for helicopter rotors, as are parabolically swept and tapered tips for propellers. More sophisticated studies of such tips are, therefore, highly recommended. CFD analyses are an obvious approach, but they would require experimental validation. A more refined tip-vortex model could then be developed for CAMRAD II (or any other wake model).

Acknowledgements

The author wishes to express his appreciation to Randy Peterson for recovering the JVX Phase II airplane-mode data, and to Wayne Johnson for his patient assistance in planning and conducting the research.

References

1. Johnson, W., Yamauchi, G. K., and Watts, M. E., "NASA Heavy Lift Rotorcraft Systems Investigation," NASA TP-2005-213467, September 2005.
2. van Aken, J. M. and Sinsay, J. D. "Preliminary Sizing of 120-Passenger Advanced Civil Rotorcraft Concepts," American Helicopter Society Vertical Lift Aircraft Design Conference, San Francisco, CA, January 2006.
3. Acree, C. W., "Impact of Technology on Heavy Lift Tiltrotors," American Helicopter Society 62nd Annual Forum, Phoenix, AZ, May 9-11, 2006.
4. Acree, C. W., "Calculation of J VX Proprotor Performance and Comparisons with Hover and High-Speed Test Data," American Helicopter Society Specialist's Conference on Aeromechanics, San Francisco, CA, January 2008.
5. Liu, J., Paisley, D. J., and Hirsh, J., "Tiltrotor Aerodynamic Blade Design by Numerical Optimization Method," American Helicopter Society 46th Annual Forum, Washington, D.C., May 1990.
6. McCarthy, T. R., Chattopadhyay, A., Talbot, P. D., and Madden, J. F., "A Performance Based Optimization of High Speed Prop-Rotors," Journal of the American Helicopter Society, Vol. 40 No. 3, July 1995.
7. Felker, F. F., Signor, D. B., Young, L. A., and Betzina, M. D., "Performance and Loads Data From a Hover Test of a 0.658-Scale V-22 Rotor and Wing," NASA TM-89419, April 1987.
8. Felker, F. F., "Results from a Test of a 2/3-Scale V-22 Rotor and Wing in the 40- by 80-Foot Wind Tunnel," American Helicopter Society 47th Annual Forum, Phoenix, AZ, May 1991.
9. Johnson, W., "CAMRAD II Comprehensive Analytical Model of Rotorcraft Aerodynamics and Dynamics," Johnson Aeronautics, Palo Alto, CA, 2007.
10. Johnson, W., "Influence of Wake Models on Calculated Tiltrotor Aerodynamics," American Helicopter Society Aerodynamics, Acoustics, and Test and Evaluation Technical Specialists Meeting, San Francisco, CA, January 2002.
11. Corrigan, J. J., and Schillings, J.J., "Empirical Model for Stall Delay Due to Rotation," American Helicopter Society Aeromechanics Specialists Conference, San Francisco, CA, January 1994.
12. Du, Z., and Selig, M.S., "A 3-D Stall-Delay Model for Horizontal Axis Wind Turbine Performance Prediction," AIAA Paper 98-0021, January 1998.
13. Jenks, M. D., and Narramore, J. C., "Final Report for the 2-D Test of Model 901 Rotor and Wing Airfoils (BSWT 592)," Bell-Boeing Report No. D901-99065-1, May 1984.
14. Acree, C. W., Jr., "A CAMRAD II Model of the V-22 Rotor for Whirl-Flutter Analysis," NASA/TM-2004-212801, July 2004.
15. Narramore, J. C., Platz, D. A., and Brand, A. G., "Application of Computational Fluid Dynamics to the Design of the BA 609," 25th European Rotorcraft Forum, Rome, Italy, September 1999.
16. Kocurek, J. D., and Tangler, J. L., "A Prescribed Wake Lifting Surface Hover Performance Analysis," American Helicopter Society 32nd Annual Forum, Washington, D.C., May 1976.
17. Narramore, J. C., "Airfoil Design, Test, and Evaluation for the V-22 Tilt Rotor Vehicle," American Helicopter Society 43rd Annual Forum, St. Louis, MO, May 1987.
18. Farrell, M. K., "Aerodynamic Design of the V-22 Osprey Proprotor," American Helicopter Society 45th Annual Forum, Boston, MA, May 1989.
19. Dadone, L., Liu, J., Wilkerson, J., and Acree, C. W., "Proprotor Design Issues for High Speed Tiltrotors," American Helicopter Society 50th Annual Forum, Washington, D.C., May 1994.
20. Johnson, W., *Helicopter Theory*, Princeton University Press, 1980.

Appendix: Ideal Twist Distributions

Following Ref. 19, the ideal twist distribution can be defined as

$$\tau = \alpha_z + \tan^{-1}\left[\left(\mu + v_i/V_{tip}\right)/(r/R)\right]$$

From Ref. 20, local induced velocity v_i can be estimated as

$$v_i = \frac{v_0(\Omega r)^2}{(\Omega r)^2 + (V + v_0)^2}$$

where

$$v_0 = \frac{\sqrt{V^2 + 4v_h^2} - V}{2} \text{ and } v_h = \sqrt{T/2\rho A}$$

Applied to JVX hover and cruise design conditions, these relations yield the curves in Fig. 34. Twist is here indexed to zero at $0.75 R$. In principle, v_i could be corrected by the κ_λ factors for hover and cruise, but the differences for the JVX rotor are negligible at the scale of Fig. 34.

The actual JVX twist is also plotted in Fig. 34. Its inboard twist rate approximates that for ideal hover twist, but its outboard rate is a compromise between cruise and hover.

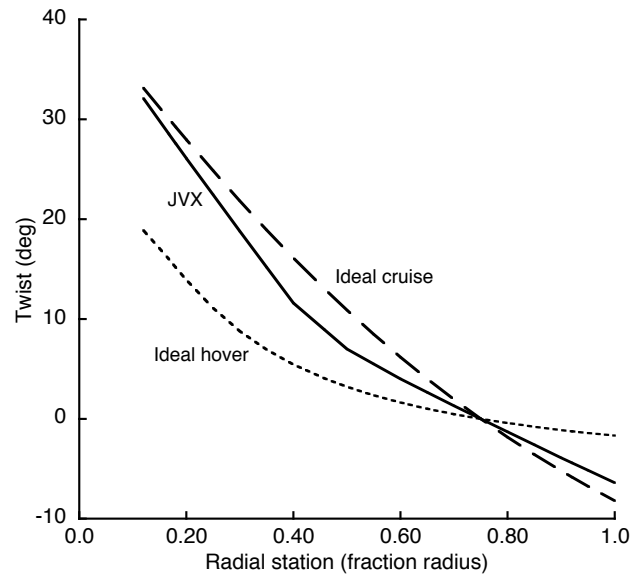


Fig. 34. Ideal and bilinear twist distributions.